CONTROL AND IDENTIFICATION OF VORTEX WAKES *

C. R. Anderson
Department of Mathematics
University of California, Los Angeles 90095-1555
anderson@math.ucla.edu

Y.-C. Chen and J. S. Gibson
Mechanical and Aerospace Engineering
University of California, Los Angeles 90095-1597
yencheng@seas.ucla.edu, gibson@seas.ucla.edu

ABSTRACT

In this paper, control and identification methods for vortex wakes are investigated. The particular problem studied concerns the stabilization of vortices behind a flat plate, using backside suction as an actuator. The flow dynamics are modeled with a discrete vortex method. Feedback control results for a linear PI controller are presented as well as identification results for a class of input/output models that can be used to design more sophisticated controllers.

1 INTRODUCTION

Active control of fluid flows has attracted wide interest in recent years (Bushnell, 1992; Gad-el-Hak, 1991; Gunzburger, 1995). The control of flow past bluff bodies has applications in drag reduction, lift enhancement, and noise and vibration control. For example, Saffman (Saffman, 1997) has suggested that by controlling vortices behind a slender body, the lift force can be increased without greatly increasing the drag force. This paper concerns the development of identification and control methods for vortex wakes, particularly wakes generated by objects with sharp edges.

The model problem considered here is the stabilization of vortices behind a flat plate with backside suction as an actuator. In the case of constant free-stream velocity, vortex shedding occurs and a vortex wake forms behind the plate. The paper demonstrates the feasibility of using feedback control in this problem by applying a constant-gain linear feedback to trap the vortices and inhibit shedding when there is no disturbance to the flow field. Most real flow-control applications involve time-varying free-stream velocities and unmodeled disturbances, and these will require more sophisticated controllers. Hence, the paper also investigates the identification of input/output models that can be used to design such controllers. The class of models identified here are especially appropriate for adaptive control, which was used in (Anderson, 1993; Chang, 1994) to reduce oscillations in vortex wakes.

The flow dynamics are modeled using a vortex blob method. In this method the evolution of the vorticity in the wake is approximated by evolving a collection of discrete vortices. The vortex shedding phenomenon (the principal viscous effect) is modeled by employing a dynamic Kutta condition (Cortelezzi, 1993). As discussed in a number of previous papers (Cortelezzi, 1993; Cortelezzi, 1996; Sarpkaya, 1975; Sarpkaya, 1979) vortex methods provide a description of the dynamics as a model with far fewer dimensions than direct numerical simulation. This reduced dimensionality makes vortex methods particularly attractive as simulations to supply approximate dynamics for the task of developing identification and control procedures. However, in order to make the vortex model suitable for identification and control, it was necessary to modify the standard discrete vortex method. Modifications that we employed include an adaptive time-stepping scheme, vortex merging, and a procedure for reducing the noise in velocity measurements near the plate.

The results of this paper illustrate that with appropriate modifications, discrete-vortex models can be quite useful for control design and simulation. In particular, the agreement found in this paper between the discrete-vortex model and the identified input/output model with respect to the minimum phase and nonminimum phase characteristics of the flow field indicates that the identified input/output models obtained from the discrete-vortex model capture the characteristics of the flow that are important in control system design.

*THIS RESEARCH WAS SUPPORTED BY AFOSR GRANT F49620-96-1-0327.

2 DISCRETE VORTEX METHOD

The problem we consider concerns the wake generated by flow about a flat plate. In our calculations, the plate has length $4a$, its midpoint is at $(0,0)$, and the plate is perpendicular to the free stream velocity $U_\infty(t)$. For this paper, we use $a = 1$. A velocity sink (suction actuator) is located at the center of the back side of the plate (i.e., at $(0^+,0)$).

To facilitate the calculation of the velocities, we use conformal mapping (Batchelor, 1967). The velocities in our problem are first computed in the mapped plane (ζ plane) and then transformed back to the physical plane (z plane). A circle in the mapped plane with center at $(0,0)$ and radius a is associated with the plate in the physical domain by the conformal transformation

$$z = \zeta - \frac{a^2}{\zeta}. \tag{1}$$

The relationship between physical and mapped planes is shown in Figure 1.

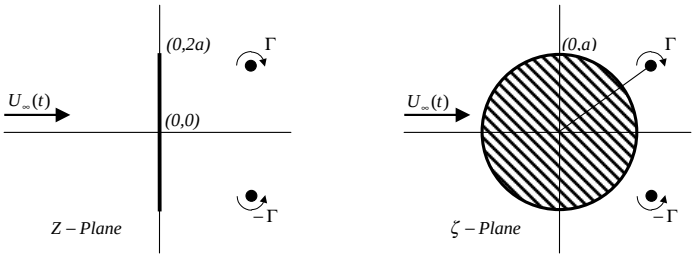

Figure 1. The mapping between physical (z-plane) and mapped plane (ζ-plane) for the flow past a flat plate.

A stream function Ψ has the same value for the corresponding points in both planes. Therefore, velocities in the physical and mapped planes can be written as

$$z-\text{plane}: \quad v(z) = i\frac{d\bar{\Psi}}{dz}; \qquad \zeta-\text{plane}: \quad v(\zeta) = i\frac{d\bar{\Psi}}{d\zeta}. \tag{2}$$

By the chain rule,

$$v(z) = i\frac{d\bar{\Psi}}{dz} = i\frac{d\bar{\Psi}}{d\zeta}\frac{d\zeta}{dz} = \frac{d\zeta}{dz}v(\zeta). \tag{3}$$

Since the mapping is singular at the plate tips ($\frac{d\zeta}{dz} = \infty$), the velocity field in the physical domain will be infinite unless the corresponding velocity in the mapped plane vanishes. In general, the Kutta condition is the requirement that the velocity field be nonsingular. In potential flow, the Kutta condition is satisfied by choosing an appropriate circulation. In the discrete vortex simulation used here, the circulation is fixed, and the Kutta condition is satisfied by choosing the strengths of newly introduced vortices so that the velocity in the mapped plane vanishes at the images of the plate tips. This approach has been used in previous vortex simulations (Chein, 1988; Sarpkaya, 1975; Sarpkaya, 1979). We follow most closely the implementation of Cortelezzi (Cortelezzi, 1997), with some modifications for initial vortex placement (Chen, 1997).

As the flow evolves, vortex sheets emanate from the tips of the plate. The vortex sheets are modeled by a collection of discrete vortices, each vortex having a prescribed circulation $\Gamma_i(t)$ and location $\zeta_i(t)$. The evolution of the sheet in regions away from the tips is treated as an inviscid evolution and so the differential equation describing the motion of the vortex centers (derived from Euler's equations) is given by

$$v_i(\zeta) = \frac{d\zeta_i(t)}{dt} = v_p(\zeta_i, t) + \sum_{i \neq j} \frac{i\Gamma_i(t)(\bar{\zeta}_i - \bar{\zeta}_j)}{2\pi|\zeta_i - \zeta_j|^2}. \tag{4}$$

Here $v_p(\zeta_i, t)$ is the sum of the potential flow velocities induced by the sink and the prescribed velocity $U_\infty(t)$. To avoid the problems caused by large velocities occurring when two vortices are in close proximity, the formula (4) is slightly modified; we use the velocity field associated with a vortex blob approximation (Chorin, 1973; Chorin and Bernard, 1973).

In the region near the plate tips, viscous effects are approximated by introducing vortex elements at each time step to simulate the separation of the viscous boundary layer into the flow field. At the beginning of each integration step, a new vortex is placed near each tip, at a location depending on the average velocity near the tip. The strengths of these new vortices are prescribed so that the Kutta condition is satisfied. Figure 2 shows streamlines for the simulation of the flow past a flat plate. That the streamlines are tangent to the plate at the tips is a result of the Kutta condition.

One feature of this vortex model is that a pair of discrete vortices is introduced at each time step. Thus, a large number of discrete vortices are generated when simulating several vortex shedding cycles (e.g., a simulation that is required to assess the open-loop behavior of the system). Since the work to compute one velocity field evaluation is $O(N^2)$ (N=the number of vortices), the computational time increases greatly. To reduce this computational time we implemented a variable time step integrator for the differential equations and a vortex merging procedure (Cortelezzi,

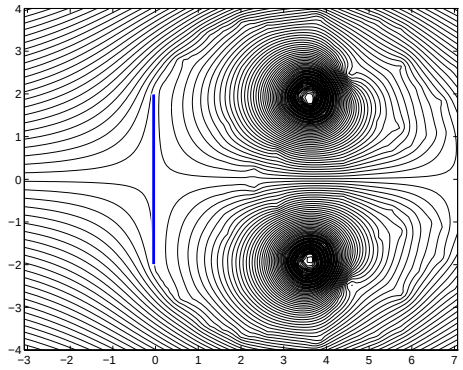

Figure 2. Instantaneous streamlines for the flow past a flat plate.

1993) to reduce the number of vortices in the calculation. These two enhancements reduced the computational time to acceptable levels. Specifically, the vortex simulations for the control and identification problems in this paper used between 300 and 700 discrete vortices (with two states per discrete vortex). A flowchart depicting the evolution of the vortex dynamics within one control time step is given in Figure 3. Here, t_k is the time at the beginning of the k^{th} control time step, Δ is the length of the sample-and-hold step for control ($t_{k+1} = t_k + \Delta$), and Δ_{RK} is the integration step, which is a variable ($\Delta_{RK} \leq \Delta$). (See (Chen, 1997) for details)

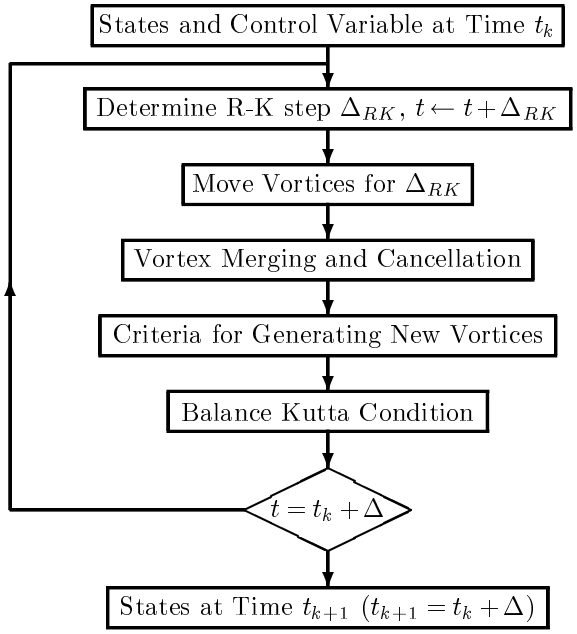

Figure 3. Flow chart for discrete vortex scheme with variable step size.

3 MEASUREMENTS

Our identification and control work required an output measurement from the vortex simulation. In order to compare our results with those of Cortelezzi (Cortelezzi, 1993; Cortelezzi, 1996), we used the center of circulation and the total circulation. The position of the center of circulation in the mapped plane is defined by

$$\zeta_c^{(k)} = \frac{1}{\Gamma_c^{(k)}} \sum_{i=1}^{N/2} \Gamma_i \zeta_i \quad \begin{pmatrix} k=1: \text{top} \\ k=2: \text{bottom} \end{pmatrix}. \tag{5}$$

The center of circulation in the physical plane, $z_c^{(k)}$, can be obtained by conformal mapping. The total circulation $\Gamma_c^{(k)}$ is defined by

$$\Gamma_c^{(k)} = \sum_{i=1}^{N/2} \Gamma_i, \tag{6}$$

where Γ_i is the strength of the i^{th} discrete vortex.

For feedback control and system identification, we took the system outputs to be velocity measurements at several points in the flow field downstream of the plate. For velocity measurement points near the plate, a characteristic feature of our vortex method is that the velocity signal is very noisy. A typical velocity signal is indicated by the dashed line in Figure 4. Several standard spatial and time domain filtering techniques were explored, but in general they proved unsatisfactory. We found that a satisfactory solution was to use the velocity induced by a pair of vortices located at the centers of circulation (essentially using the velocity induced by a pair of vortices that are amalgamations of all the vortices). In terms of the total circulation Γ_c and the center of circulation ζ_c the complex conjugate of this velocity is given by

$$\bar{v}(\zeta) = w = \frac{d\Psi}{d\zeta} = U_\infty(t)(1 - \frac{1}{\zeta^2}) + S\frac{\zeta+1}{\zeta(\zeta-1)} + \sum_{k=1}^{2} \frac{i\Gamma_c^{(k)}}{2\pi} \left(\frac{1}{\zeta - \zeta_c^{(k)}} + \frac{\bar{\zeta}_c^{(k)}}{1 - \zeta\bar{\zeta}_c^{(k)}} \right). \tag{7}$$

The solid line in Figure 4 shows the value of this velocity measurement, which we call the modified velocity measurement. As Figure 4 shows, the modified velocity measurement is much less noisy than the unfiltered velocity measurement, and hence a better system output for use in the PI controller in Section 5.

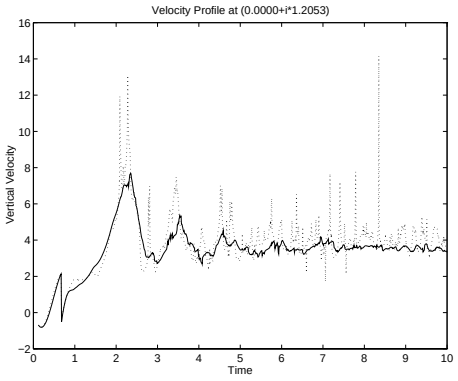

Figure 4. Comparison between unfiltered velocity measurement (dashed line) and the modified velocity measurement (solid line) on the downstream wall.

4 FLOW DESCRIPTION AND CONTROL PROBLEM

The uncontrolled flow is shown in Figure 5(a) and is characterized by the formation of vortex street. The vortex shedding causes unsteady drag forces to be exerted upon the plate. In an effort to reduce these unsteady forces, the control problem becomes one of trying to trap the vortices behind the plate and thus inhibit the vortex shedding process. Suction on the centerline of the downstream side of the plate is used as an actuator.

The possibility that the vortices can be trapped and vortex shedding inhibited is demonstrated in Figure 5(b), where we show the results of applying an open-loop constant control. In general, the amount of suction necessary to trap the vortices when there is non-constant free stream velocity and/or unmodelled disturbances is not known, therefore closed-loop control strategies capable of determining the appropriate suction are desired.

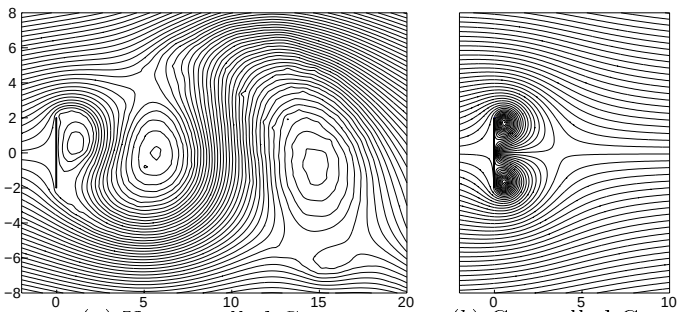

(a) Uncontrolled Case (b) Controlled Case

Figure 5. Instantaneous streamlines for flow past a flat plate.

The free-stream velocity used in our study is shown in Figure 6. This velocity consists of an initial disturbance of finite duration followed by a constant value. The initial perturbation accelerates the formation of large vortical structures behind the plate and enhances the process of vortex shedding and reformation.

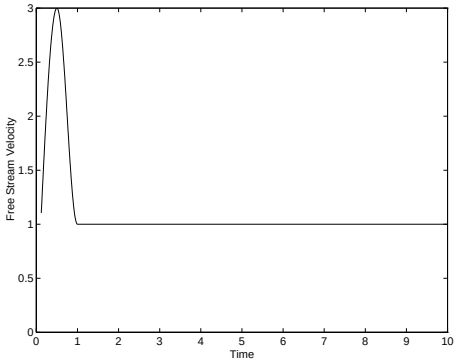

Figure 6. Free Stream Velocity.

By using an idealized point vortex model of this flow problem, Cortelezzi (Cortelezzi, 1997) developed a nonlinear controller which performed very well in the case of constant and sinusoidal free stream velocity. This controller, with suitable modifications, was applied successfully to a discrete vortex simulation similar to the one used here (Cortelezzi, 1997; Chen, 1997). However, in an effort to avoid the use of controllers designed with a complete (analytic) knowledge of the system dynamics, as well as controllers that require non-physical input measurements, we began the investigation of linear feedback controllers based on identified input-output models.

5 LINEAR PI CONTROLLER

The starting point for our control investigations is the implementation of a linear PI controller to stabilize the vortices behind the plate in the case when the free stream velocity has the profile given in Figure 6.

For PI Control, the measured output is v, the modified velocity at a point on the downstream wall. (This velocity is vertical.) The desired output is a constant v_d. We take $\epsilon = v_d - v$ as the input to the controller.

$$S_m = -K_P \epsilon_m - K_I \sum_{i=1}^{m} \left[\frac{\epsilon_i + \epsilon_{i-1}}{2} h \right], \qquad (8)$$

where m denotes the time step, S_m is the control suction for the m^{th} control interval, $\epsilon_i = v_d - v_i$ with v_i the output

at the i^{th} time step, and h is the length of the time step. Also, K_P is the proportional gain and K_I is the integral gain. To reduce the computation effort for each time step, the following recursive form is used:

$$S_m = S_{m-1} - (K_P + K_I \frac{h}{2})\epsilon_m - (-K_P + K_I \frac{h}{2})\epsilon_{m-1}. \quad (9)$$

In our study, h is chosen to be 0.01, and K_P and K_I are two constants that must be determined. In order to compare our control results with Cortelezzi's nonlinear controller (Cortelezzi, 1997), the linear PI controller was activated when the rate of circulation production first changed sign.

The measured output from the system consists of a modified velocity measurement (as described in Section 3) located at $z = (0^+, 1.9237)$. (Since the width of the plate is 4, the coordinates of the top tip are $z = (0, 2)$.) In an open-loop test with suction $S = -1.4$, one finds that the vortices are stabilized and the average modified velocity at the measurement point is 4.5.

Using the modified velocity measurement $v_d = 4.5$ as a target output and the free stream velocity profile of Figure 6, we found the linear PI controller quite capable of determining an appropriate suction value to stabilize the vortices. (In this case $K_P = -0.2$ and $K_I = -10.0$.) Figure 7 shows the trajectory of the center of circulation for the top vortices, along with the time histories of the horizontal coordinate X_top of the center of circulation, the suction strength, and the total circulation. The time average velocity measurement from $t = 8$ to $t = 10$ is shown in Table 1.

	$z_c^{(1)} = (X\_top, Y\_top)$	$\Gamma_c^{(1)}$
Open-Loop	$(0.57, 1.64)$	20.11
Closed-Loop	$(0.57, 1.65)$	20.19
	S	$\langle v \rangle$
Open-Loop	$-1.40(constant)$	4.50
Closed-Loop	-1.42	4.50

Table 1. Time averages (from $t = 8$ to $t = 10$) of the results shown in Figure 7: $z_c^{(1)}$ = center of circulation (Top), $\Gamma_c^{(1)}$ = total circulation (Top), S = suction strength, v = velocity measurement.

We also applied the linear PI controller with the measurement being either the center of circulation or the total

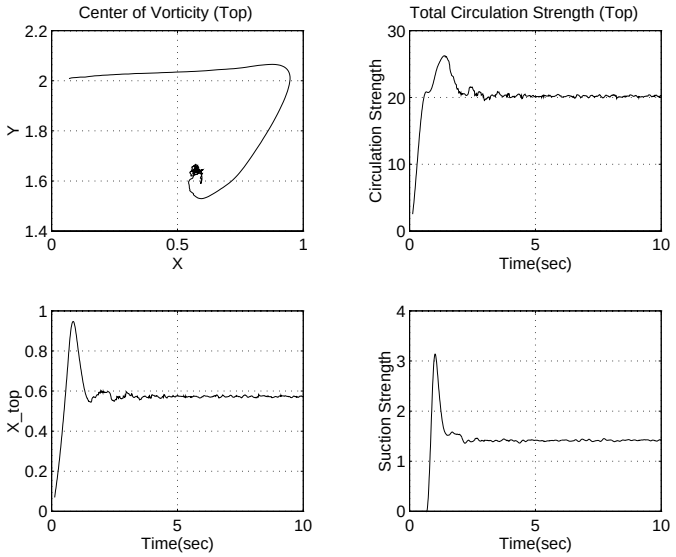

Figure 7. The simulation result of the linear PI controller with the modified velocity measurement on the downstream wall as measurement.

circulation. In both cases, we found results similar to those with the modified velocity measurements: the controller was able to determine the appropriate value of suction to achieve the target output measurement and stabilize the large vortices. (See (Chen, 1997) for details.) These and other experiments indicate that a linear PI controller performs satisfactorily when the free-stream velocity is perturbed by a disturbance of limited duration.

In the case of a sinusoidal free stream velocity, the linear PI controller was able to trap vortices behind the plate, but the measured output, as well as the center of circulation and total circulation, contained significant oscillations. This result is not unexpected because the linear PI controller, unlike the nonlinear controller proposed by Cortelezzi, carries no information about the dynamics of the flow. To reduce the amplitude of such oscillations, a more sophisticated controller will be needed. The first step towards developing such controllers is the identification of input-output models of the system. This is addressed in the remaining sections of the paper.

6 SYSTEM IDENTIFICATION AND FREQUENCY RESPONSE

Vertical velocity measurements (unmodified) at points on the downstream side of the plate form the basis for our system identification. The locations of the measurement points are chosen in the mapped plane in the range of $r = (1, 2, 3, 4)$ and $\theta = \frac{\pi}{2} - (\frac{k}{34})\pi$, $(k = 1, 2, \ldots, 16)$. The point

numberings and corresponding positions in the plate plane are shown in Figure 8.

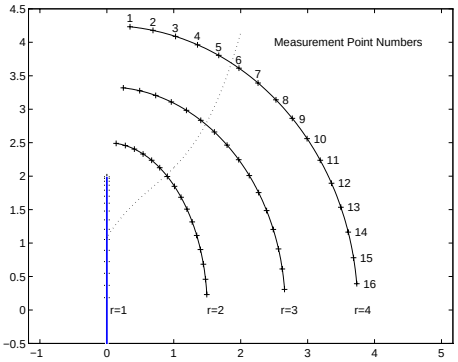

Figure 8. The position and numbering of the measurement points in Z-plane. (The dashed line shows the locus of the intersection points discussed in Section 7.1.)

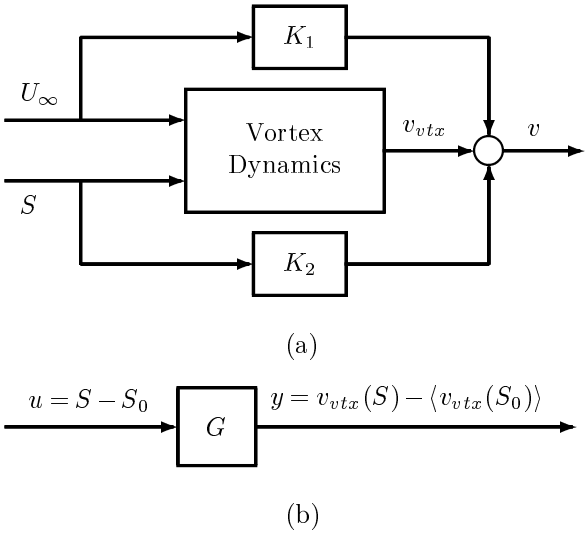

Figure 9. The relationship between input $u = S - S_0$, and output $y = v_{vtx}(S) - \langle v_{vtx}(S_0)\rangle$.

As shown in Figure 9(a) and 9(b), the vertical velocity measurement, denoted by v, has contributions from the free stream velocity, the suction, and the vortex dynamics. Thus, in the vertical velocity measurement, both the free stream velocity and the suction not only affect the measurement through movement and strength variation of the vortices, but also contribute to the measurement directly as shown in Figure 9(a). In our study we found it useful to remove these direct feed through terms and use the remaining velocity as our measurement, or system output. Thus, we decompose the vertical velocity as

$$v = K_1 U_\infty + K_2 S + v_{vtx} \tag{10}$$

where $K_1 U_\infty$ and $K_2 S$ are the contributions to the vertical velocity component from potential flow past the plate with horizontal free-stream U_∞ in the far field and suction S at the mid point on the back side of the plate. The DC gains K_1 and K_2, which depend upon the location of the measurement point, can be obtained from potential-flow theory. The remaining term v_{vtx} in (10) represents the portion of the vertical velocity due to the vortex dynamics.

In Figure 9(b) and throughout this paper, the notation $\langle \cdot \rangle$ means the time average of a quantity. Also, $v_{vtx}(S)$ denotes the output of the vortex simulation corresponding to a suction of strength S.

The full dynamics of the flow are too nonlinear to be represented by a single linear input/output model, so we chose to identify a linear input/output model for perturbations from a nominal steady-state flow. The nominal flow was produced by a constant nominal suction $S_0 = -1.5$. We identified the transfer function G in Figure 9(b), which is the mapping from the input $u = S - S_0$ to the output $y = v_{vtx}(S) - \langle v_{vtx}(S_0)\rangle$. In other words, G is the transfer function from perturbations in the suction S to perturbations in the velocity measurement v_{vtx}. To produce the input/output data for identification, we excited the vortex simulation by taking the input sequence u as a white-noise sequence with mean 0 and variance 0.2.

The identified discrete-time input/output model has the form of the ARX (auto-regressive with exogenous input) model

$$y(t) + \sum_{i=1}^{n} a_i y(t-i) = \sum_{i=1}^{n} b_i u(t-i), \tag{11}$$

where the coefficients a_i and b_i are determined by a least-squares fit to the data. We used the MATLAB ARX function to identify the coefficients in the ARX model of each order n from 3 to 30.

The next task was to determine the order n for which the ARX model best represents the input/output properties of the system being identified. Typically, one incrementally increases the order of the model, and hopes that the Bode plots show convergence after a particular order. Such convergence did not occur for our system. We believe that this is due to the inherent non-linearity of the plant.

We then used the following systematic approach to determine the optimal ARX order. The idea is to run a series of discrete vortex simulations with single-frequency si-

nusoidal inputs and choose the ARX order for which the frequency response of the model most closely matches the frequency response of the simulation. By using a series of 33 input frequencies f_i, we obtain a series of sinusoidal outputs. For each input frequency, the ratio of output amplitude to input amplitude for the vortex simulation is A_i, and the relative phase between input and output is ϕ_i. These amplitudes and phases are shown by the asterisks in Figure 11, for measurement point 10 ($r = 3$).

To determine the optimal ARX model order n, we select the order of the ARX model whose frequency response closest in the L_2 sense to the frequency response of the vortex simulation. To do this, we minimize the fit-to-data criterion

$$J = \sum_{i=1}^{N_f} |\hat{A}(f_i)e^{i\hat{\phi}(f_i)} - A_i e^{i\phi_i}|^2 \qquad (12)$$

where $N_f = 33$ for the results presented here. Figure 10 shows the fit-to-data criterion J with different model orders at points 6 and 10 ($r = 3$). The model order n that minimizes J at each measurement point with $r = 3$ is shown in Table 2. At all measurement points, the fit-to-data criterion J is similar to the plots in Figure 10(b); in particular, there always is a minimum value at some order $n < 30$.

Point Number	1	2	3	4	5	6	7	8
Optimal Order	6	4	5	5	3	3	5	4
Point Number	9	10	11	12	13	14	15	16
Optimal Order	5	5	5	5	5	9	7	6

Table 2. The optimal model orders at measurement points downstream of the plate ($r = 3$).

The result of the system identification using the optimal order ($n = 5$) at point 10 is shown in Figure 11. Amplitude and phase responses corresponding to single-frequency inputs are shown by asterisks. The amplitude matches very well, and the phase matches very well at low frequency. At frequencies around half the Nyquist frequency, the phase shows significant errors. However, because the amplitude is very small in this frequency range, these phase errors do not represent a significant difference between the frequency response of the vortex simulation and the frequency response of the ARX model.

We tested our identification procedure without removing the mean value of the I/O signals and were not able to get credible identification results. Thus, as expected, linearization about a nominal operating condition is crucial for identification of systems governed by nonlinear dynamics.

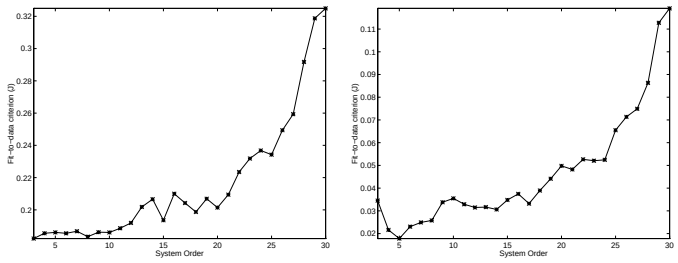

(a) Point Number 6 (b) Point Number 10

Figure 10. Fit-to-data criterion J for model orders $n = 3, \ldots, 30$ at points 6 and 10.

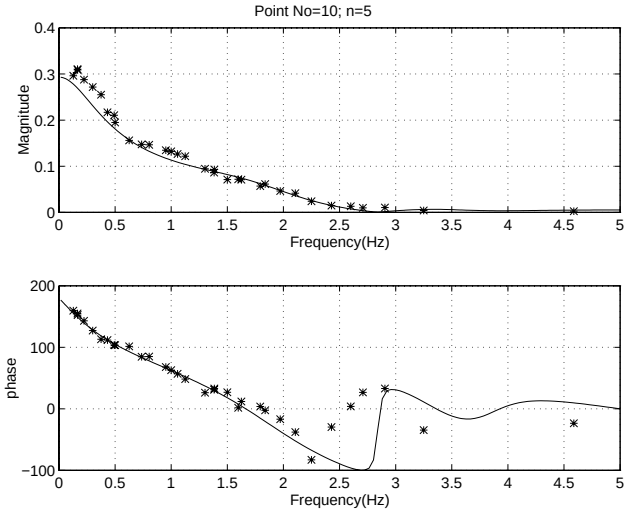

Figure 11. Bode plots for the vortex simulation (*) and the identified ARX model of order 5 (solid lines); Point Number 10.

7 TIME-DOMAIN RESPONSE

In this section, we evaluate the identified ARX model by comparing its DC gain and step response to those of the discrete-vortex model. The DC gain and step response of the discrete vortex simulation are readily obtained, and are two of the most important characteristics of the time-domain response of any control system. The order of the ARX model used here was the optimal order selected as discussed in the preceding section.

7.1 COMPARISON OF DC GAINS

7.1.1 DC Gain of the Discrete Vortex Model A series of vortex simulations were performed with $U_\infty = 1.0$ and constant suctions $S = \{-1.0, -1.1, -1.2, \ldots, -2.0\}$ chosen as inputs. The mean modified vertical velocities, $\langle v_{vtx} \rangle$, at different measurement points in the physical plane (Figure 8 and $r = 3$ and $r = 4$) are shown in Figure 12. The results for constant suction equal to -1.5 are shown in dashed lines.

One notices that even though the differences in the inputs are uniform (in our case, $\Delta S = 0.1$), the gaps between the curves are not uniform. This result demonstrates that the dynamics of the vortex simulation is nonlinear. The non-linearity can be inferred from the behavior of the trapped vortical structures as suction is applied. With suction, these vortical structures do not move rigidly; the presence of the plate causes them to deform. This deformation introduces non-linearity in the measured velocity.

An additional interesting feature of the DC gain curves is the presence of a particular point at which all of the curves intersect. This point (which we refer to as the intersection point) occurs between points in 6 and 7 in Figure 12(a), between points 5 and 6 in Figure 12(b). Analysis of the corresponding plots for different values of r reveals a definite trend for the location of the intersection points. The locus of these intersection points is shown by the dotted line in Figure 8. Currently, an explanation of this feature alludes us; however, the change in character of the step response near these points (as will be discussed in section 7.2) has motivated current investigation.

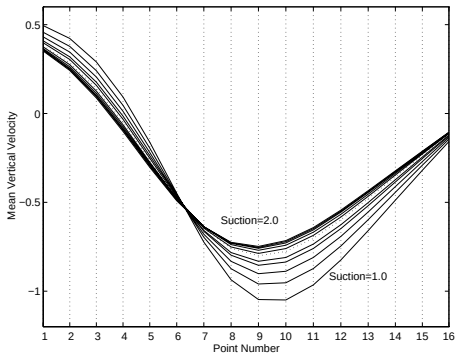

(a) $r = 3$

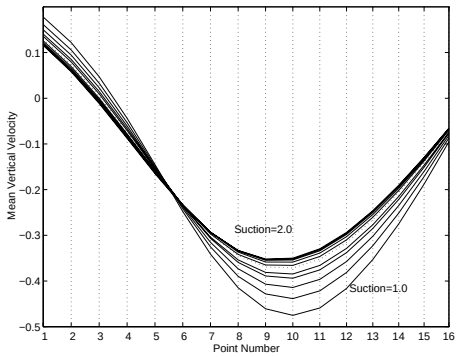

(b) $r = 4$

Figure 12. Mean velocity measurement on the downstream side of the plate.

7.1.2 DC Gain of the ARX Model In Figure 13, Curve A shows the DC gain of the ARX model of optimal order (table 2) identified at each of the 16 measurement points ($r = 3$, Figure 8). These ARX models approximate the relationship between a perturbation from the nominal constant suction $S_0 = -1.5$ and the resulting perturbation in the measured output. Hence, the DC gain of each identified ARX model is the value predicted by that ARX model for the ratio

$$\frac{\langle v_{vtx}(S) \rangle - \langle v_{vtx}(S_0) \rangle}{S - S_0}, \tag{13}$$

where $\langle v_{vtx}(S) \rangle$ is the mean value of the velocity measurement from the vortex simulation when the suction S is constant.

Figure 13 compares the DC gain of the identified ARX model at each measurement point to the corresponding values of the ratio in (13) for $S - S_0 = +0.5$ (Curve B) and for $S - S_0 = -0.5$ (Curve C). Curve B, for example, is the difference between the curves in Figure 10(c) for suctions of -1.0 and -1.5, scaled by $1/(+0.5)$. Since the identified ARX model is linear, its prediction of the ratio in (13) is symmetric with respect to $S - S_0$; however, the actual ratio, which is computed from the nonlinear vortex simulation, is not symmetric in $S - S_0$, as evidenced by the fact that Curves B and C are different. It should be expected that the least-squares algorithm will produce some average of Curves B and C by identifying ARX models with DC gains that fall between Curves B and C. This is the case everywhere except at points 6 and 7, where Curve A is very near one of the other curves. With the limitations inherent in fitting a linear model to a nonlinear system, the results in Figure 13 are the best that can be expected.

7.2 STEP RESPONSE

Here we examine step responses for measurement points 3, 6, and 10 ($r = 3$). Figures 14(a), 14(b), and 14(c) show step responses of the vortex simulation at the measurement points indicated, while Figures 14(d), 14(e), and 14(f) show the corresponding step responses of the identified ARX models of optimal orders. The step input is a sudden change in suction, from the initial constant suction

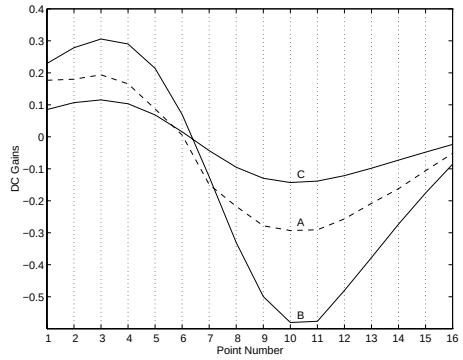

Figure 13. The relationships between the DC gains of the vortex simulation and the identified ARX model ($r = 3$). Curve A: DC gains of ARX model; Curve B: ratio in (13) from vortex simulation with $S_0 = -1.0$, $S = -1.5$; Curve C: ratio in (13) from vortex simulation with $S_0 = -1.5$, $S = -2.0$.

$S_0 = -1.5$ to the new constant suction $S = -1.0$; i.e., the step is $S - S_0 = +0.5$. The corresponding perturbations in the measurement v_{vtx} from the vortex simulations are the time histories of the difference

$$v_{vtx}(S)(t) - v_{vtx}(S_0)(t), \qquad t \geq 0. \tag{14}$$

This is the output plotted in Figures 14(a), 14(b), and 14(c). The time when the suction is changed from S_0 to S is taken as $t = 0$, and $v_{vtx}(S_0)(t)$ in (14) is the velocity measurement with constant suction $S_0 = -1.5$ for all t.

In Figures 14(b), the initial responses move to negative values before recovering to positive steady-state mean values. This behavior is characteristic of non-minimum phase systems. See (Franklin, 1994; Nise, 1992). On the contrary, in Figures 14(a) and 14(c), the step responses move in one direction only, toward the steady-state values. This is characteristic of minimum phase systems.

We ran a series of simulations with the same conditions at all measurement points, ($r = 3$). The signs of the asymptotic values of the step responses are all consistent with what is shown in Figure 12. From points 1 to 6, when a step input is applied, the steady-state vertical velocity increases. From points 7 to 16, the steady-state vertical velocity decreases. The intersection point between points 6 and 7 separates these two regions. Figure 14(b) suggests that point 6 lies in a transition region.

The same step input (magnitude 0.5) was applied to the identified ARX models to obtain the results in Figure 14(d), 14(e), and 14(f). These step responses agree with those for the vortex simulation with respect to both the signs of the asymptotic values and the minimum-phase/nonminimum-phase properties. Also, for measurement points 3 and 10, as well as for most of the other points, the mean steady-state values of the step responses are consistent with the results shown in Figure 13 for DC gains.

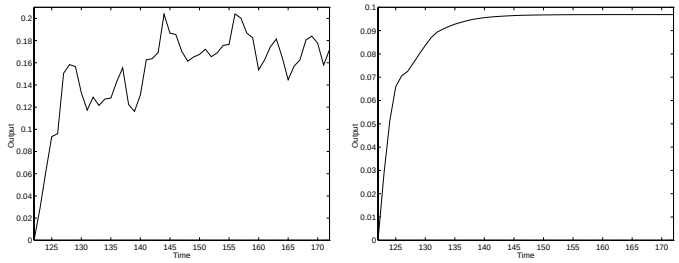

(a) Flow simulation (Point number 3)

(d) Identified model (Point number 3)

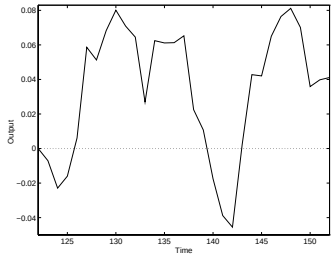

(b) Flow simulation (Point number 6)

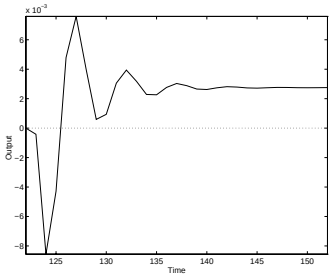

(e) Identified model (Point number 6)

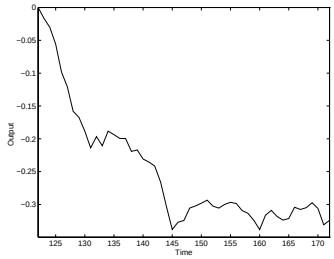

(c) Flow simulation (Point number 10)

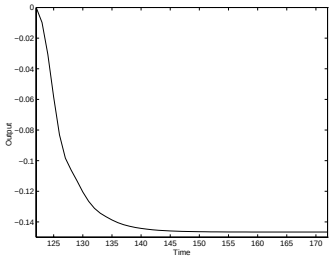

(f) Identified model (Point number 10)

Figure 14. Comparison between the step responses of the vortex simulation and the identified ARX models ($r = 3$).

8 CONCLUSIONS

A discrete vortex model was implemented to simulate two-dimensional flow past a flat plate with a suction point on the center line of the downstream wall. Conformal map-

ping was used to transform this problem to the conventional problem of flow around a unit circle. A "dynamic" Kutta condition determined the circulations of the vortices shed from the plate tips.

A recursive linear PI control algorithm was applied to the case of a free-stream velocity with an initial perturbation of finite duration. This PI controller was quite capable of determining an appropriate suction value to stabilize the two large vortical structures behind the plate. The PI controller results for a sinusoidal free-stream velocity were not as satisfactory. To lay the foundation for more advanced controller design, we then focused on the problem of system identification.

Through the use of a variable step discrete vortex model, we are able to obtain sufficient data for system analysis and identification. We identified ARX model's of orders 3 through 30 to describe the behavior of the vortex system about a nominal state (constant suction). The ARX model actually used to represent the system was selected by choosing that model whose frequency response best matched the frequency response of the discrete vortex system at a predefined set of frequencies.

We compared the DC gains and step responses of the ARX model and the discrete vortex simulation. The DC gains of the ARX model approximated the DC gains of the vortex simulation well. Typically, the model provided DC gains that were bracketed by the DC gains of the system. Additionally, there was very good agreement with respect to the step response. The ARX models were able to capture the change in the system from minimum phase behavior to non-minimum phase behavior as the sample point was moved.

It is well known that non-minimum phase systems are more difficult to control robustly than are minimum phase systems. Also, it is common that whether a control system is minimum phase or non-minimum phase depends on actuator and sensor locations. Thus, it should be expected that the input/output mappings for flow-control problems can be either minimum phase or non-minimum phase, depending on were in the flow field the measurements are taken. The identified models, then, have two important roles in flow control: first, to guide the placement of sensors and/or actuators; second, to serve as the models used for controller design.

The identification results reported here give us confidence that ARX models can be used to represent the behavior of the discrete vortex system about a nominal state. Current work is focused on the use of these models to design controllers that are capable of stabilizing vortices in the presence of a wide range of free-stream velocity disturbances.

REFERENCES

C. R. Anderson, H.-L. Chang, and J. S. Gibson, Adaptive control of vortex dynamics. 32nd Control and Decision Conference, IEEE, December 1993.

G. K. Batchelor, An Introduction to Fluid Dynamics. Cambridge University Press, Great Britan, 1967.

D. M. Bushnell, Longitudinal vortex control – techniques and applications. The 32^{nd} Lanchester Lecture. Aeronautical Journal 96, 293-312, 1992.

H.-L. Chang, Control of Vortex Dynamics. PhD thesis, University of California, Los Angeles, 1994.

R. Chein, and J. N. Chung, Discrete vortex simulation of flow over inclined and normal plates. Computers and Fluids, pages 405-427, 1988.

Y.-C. Chen, Control and Identification of the Flow Past a Flat Plate with Discrete Vortex Simulations. PhD thesis, University of California, Los Angeles, 1997.

A. J. Chorin, Numerical study of slightly viscous flows. Journal of Fluid Mechanics. 57, 785-796, 1973.

A. J. Chorin, and P. S. Bernard, Discretization of a vortex sheet with a example of roll-up. Journal of Computational Physics, 13:423-429, 1973.

L. Cortelezzi, A Theoretical and Computational Study on Active Wake Control. PhD thesis, California Institute of Technology, 1993.

L. Cortelezzi, Nonlinear Feedback Control of the Wake Past a Plate with a Suction Point on the Downstream Wall. Journal of Fluid Mechanics, Vol. 327, 303–324, 1996.

L. Cortelezzi, Y.-C. Chen, and H.-L. Chang, Nonlinear Feedback Control of the Wake Past a Plate: from a Low-order Model to a Higher-order Model. Physics of Fluids A, Vol. 9, (7), 2009–2022, 1997.

G. F. Franklin, J. D. Powell, and A. Emami-Naeini, Feedback control of dynamic systems. Addison Wesley, 1994.

M. Gad-el-Hak and D. M. Bushnell, Separation control: review. ASME J. of Fluids Engineering. 113, 5-30, 1991.

M. D. Gunzburger, Flow control. Springer-Verlag, New York, 1995.

B. C. Kuo, Automatic control systems. Prentice-Hall, Inc., Eaglewood Cliffs, New Jersey, 1987.

N. S. Nise, Control systems enginerring. The Benjamin/Cummings Publishing Company, Inc., 1992.

P. G. Saffman and J. S. Sheffield, "Flow over a wing with an attached Free Vortex." Studies in Applied Mathmatics, 1977, 57.

T. Sarpkaya, An inviscid model of two-dimensional vortex shedding for transient and asymptotically steady separated flow over an inclined plate. Journal of Fluid Mechanics, 68:109-128, 1975.

T. Sarpkaya, and R. L. Schoaff, Inviscid model of two dimensional vortex shedding by a circular cylinder. AIAA Journal, 17(11): 1193-1200, 1979.